



## RESEARCH LETTER

10.1002/2016GL068239

## Key Points:

- Uncertainties in mantle geophysical properties to 2000 km depth are assessed stochastically
- Uncertainty in *P* wave speed and density is greatest in the upper mantle
- Uncertainty in *S* wave speed is roughly constant with depth

## Supporting Information:

- Supporting Information S1

## Correspondence to:

J. A. D. Connolly,  
james.connolly@erdw.ethz.ch

## Citation:

Connolly, J. A. D., and A. Khan (2016), Uncertainty of mantle geophysical properties computed from phase equilibrium models, *Geophys. Res. Lett.*, 43, doi:10.1002/2016GL068239.

Received 11 FEB 2016

Accepted 13 APR 2016

Accepted article online 1 MAY 2016

## Uncertainty of mantle geophysical properties computed from phase equilibrium models

J. A. D. Connolly<sup>1</sup> and A. Khan<sup>2</sup><sup>1</sup>Institute of Geochemistry and Petrology, ETH Zürich, Switzerland, <sup>2</sup>Institute of Geophysics, ETH Zürich, Switzerland

**Abstract** Phase equilibrium models are used routinely to predict geophysically relevant mantle properties. A limitation of this approach is that nonlinearity of the phase equilibrium problem precludes direct assessment of the resultant uncertainties. To overcome this obstacle, we stochastically assess uncertainties along self-consistent mantle adiabats for pyrolytic and basaltic bulk compositions to 2000 km depth. The dominant components of the uncertainty are the identity, composition and elastic properties of the minerals. For *P* wave speed and density, the latter components vary little, whereas the first is confined to the upper mantle. Consequently, *P* wave speeds, densities, and adiabatic temperatures and pressures predicted by phase equilibrium models are more uncertain in the upper mantle than in the lower mantle. In contrast, uncertainties in *S* wave speeds are dominated by the uncertainty in shear moduli and are approximately constant throughout the model depth range.

## 1. Introduction

Since the work of Francis Birch [e.g., Birch, 1952], our ability to constrain Earth's constitution and structure from surface observations has improved due to advances in: laboratory techniques; first-principle computational methods; and geophysical data acquisition and analysis. As a consequence, we find ourselves in the advantageous position of being able to directly confront plausible geochemical and petrological models of Earth's interior with geophysical observations.

Seismological constraints on Earth's mantle composition typically derive from a comparison of seismic velocities inferred from various regional and global seismological studies with laboratory measurements of elastic properties of the relevant minerals at appropriate pressures and temperatures [Ito and Stixrude, 1992; Jackson, 1998; Ganguly et al., 2009; Murakami et al., 2012]. Because of the inherent limitations in qualitative comparisons, recent studies have sought to infer compositional and thermal parameters directly from seismic models and/or data based on geophysical properties that are computed using parameterized phase diagram approaches or thermodynamically self-consistent Gibbs energy minimization methods. Gibbs energy minimization is a technique by which mantle mineralogy, and ultimately its elastic and other thermodynamic properties, can be predicted as a function of pressure, temperature, and bulk composition from thermodynamic data. Although Gibbs energy minimization has long been advocated for geophysical problems [e.g., Saxena and Eriksson, 1983; Wood and Holloway, 1984; Sobolev and Babeyko, 1994; Kuskov and Fabrichnaya, 1994; Bina, 1998], it is only in the last decade that the availability of comprehensive thermodynamic data bases [e.g., Fabrichnaya et al., 2004; Stixrude and Lithgow-Bertelloni, 2005, 2011; Khan et al., 2006; Matas et al., 2007; Piazzoni et al., 2007] has made the application of such calculations feasible for geophysical models of the entire Earth's mantle [e.g., Mattern et al., 2005; Cobden et al., 2009; Cammarano et al., 2009; Khan et al., 2009; Afonso et al., 2013; Drilleau et al., 2013; Kuskov et al., 2014].

Although geophysical inverse methods have proven effective in optimizing profiles of mantle composition and temperature, and thus geophysical properties that match geophysical data, the uncertainties in geophysical properties computed from phase equilibrium models are difficult to assess because the nonlinearity of the phase equilibrium problem precludes simple error propagation. Here we use Monte Carlo analysis, i.e., statistical treatment, to assess these uncertainties from error estimates for the underlying thermodynamic data. In this analysis we consider the influence of each thermodynamic parameter individually. The maximum uncertainty obtained by such a conditional treatment is the minimum uncertainty associated with the

**Table 1.** Model Compositions<sup>a</sup>

Component	Pyrolite	MORB
CaO	3.1	13.05
FeO	8.0	7.68
MgO	38.3	10.49
Al <sub>2</sub> O <sub>3</sub>	3.9	16.08
SiO <sub>2</sub>	46.4	50.39
Na <sub>2</sub> O	0.03	1.87

<sup>a</sup>From Khan *et al.* [2009]. Numbers are in wt %.

thermodynamic prediction. As many thermodynamic parameters are strongly correlated [e.g., Bass *et al.*, 1981; Bina, 1995], the true uncertainty is unlikely to be substantially greater than the maximum obtained from our conditional analysis.

Uncertainty in phase equilibrium-based models of mantle properties can be decomposed into three major components: the identity of the stable minerals, the compositions of the minerals, and the elastic properties of the minerals. We distinguish these here, respectively, as the mineralogical, compositional, and elastic components of the uncertainty. Previous assessments suggest that the elastic component results in uncertainties of 0.5–1%, 1–3%, and 2–4% in, respectively, mantle density, *P* wave speed, and *S* wave speed [e.g., Kuskov and Fabrichnaya, 1994; Connolly and Kerrick, 2002; Cammarano *et al.*, 2003; Kennett and Jackson, 2009]. Several previous studies have addressed additional ways in which the assumptions of phase equilibrium modeling and/or thermodynamic uncertainties may impact geophysical interpretation [e.g., Afonso *et al.*, 2013; Kuskov *et al.*, 2014; Cammarano, 2013; Thio *et al.*, 2016]. As our goal is to isolate the phase equilibrium component of the uncertainty, we neglect uncertainty associated with factors such as anisotropy, fabric, and bulk chemical composition.

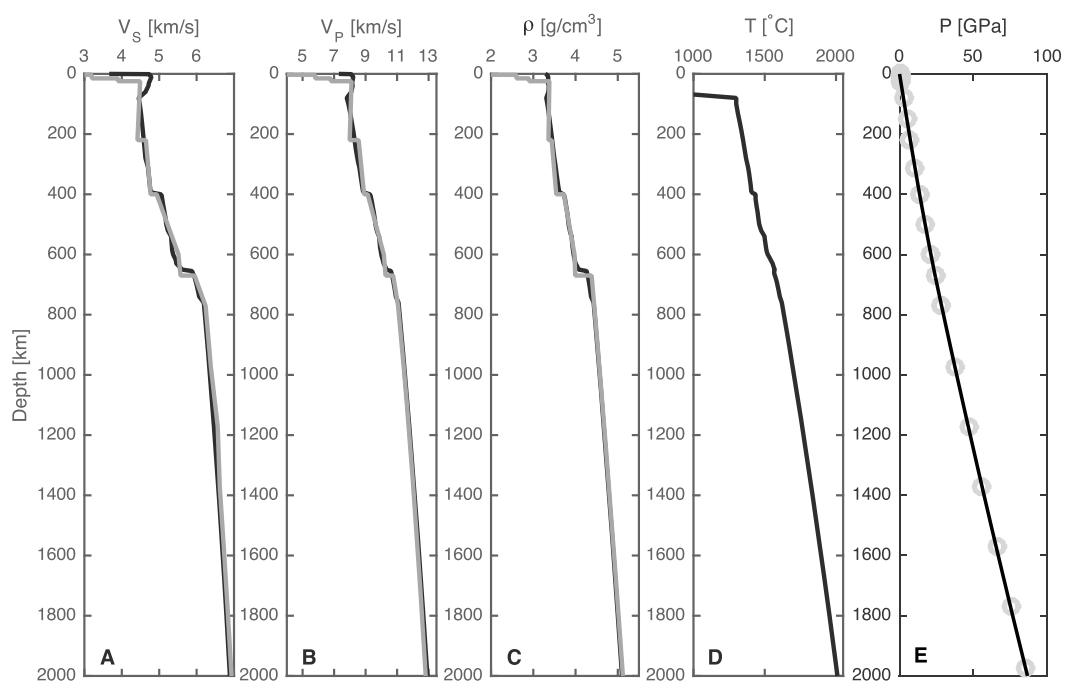


**Figure 1.** Mantle reference profiles: (a) *S* wave speed, (b) *P* wave speed, (c) density, (d) temperature, and (e) pressure as a function of depth for a pyrolitic bulk composition (Table 1) computed from thermodynamic data [Stixrude and Lithgow-Bertelloni, 2011] by Gibbs energy minimization. These properties define the reference values used to evaluate the conditional uncertainties resulting from the individual uncertainties in the various thermodynamic parameters of the model. Black lines indicate reference model values (Figures 1a–1e), and gray lines (Figures 1a–1c) and circles (Figure 1e) show corresponding Preliminary Reference Earth Model [PREM; Dziewonski and Anderson, 1981] values.

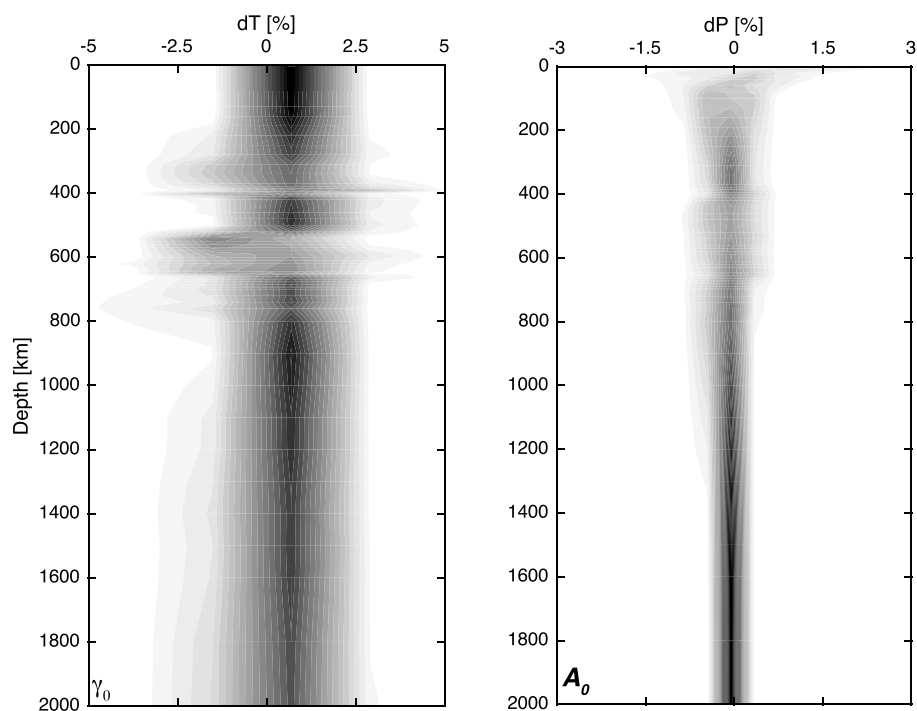


**Figure 2.** Uncertainty in temperature ( $dT$ ) and pressure ( $dP$ ) as a function of depth arising from uncertainty in, respectively, the thermodynamic parameters  $\gamma_0$  and  $A_0$ . These parameters were chosen among the 11 parameters considered because they lead to the greatest uncertainty in the self-consistent extrapolation of the mantle adiabat. Uncertainties computed relative to the reference model (Figure 1). Gray-scale levels indicate eight equally-sized probability density intervals for the distributions, with black indicating most probable and white least probable.

## 2. Analysis

We explore uncertainties in seismic wave speeds and density computed by using Gibbs energy minimization [Connolly, 2009] to predict the stable mineralogy along a self-consistent mantle adiabat for pyrolite and mid-ocean ridge basalt (MORB) bulk chemical compositions in the  $\text{Na}_2\text{O}-\text{CaO}-\text{FeO}-\text{MgO}-\text{Al}_2\text{O}_3-\text{SiO}_2$  system (Table 1). For this purpose we adopt the thermodynamic formulation of *Stixrude and Lithgow-Bertelloni* [2005] and parameters and uncertainties as given in *Stixrude and Lithgow-Bertelloni* [2011]. In this formulation, the properties of pure or end-member phases are determined by the values of 10 empirical parameters at the ambient pressure-temperature reference condition: Helmholtz energy,  $A_0$ ; volume,  $V_0$ ; Debye temperature,  $\theta_0$ ; Grüneisen parameter,  $\gamma_0$ ; the logarithmic derivative of the Grüneisen parameter with respect to volume,  $q_0$ ; isothermal bulk modulus,  $K_0$ ; pressure derivative of the bulk modulus,  $K'_0$ ; adiabatic shear modulus,  $G_0$ ; the pressure derivative of the shear modulus,  $G'_0$ ; and the shear-dependent part of the finite strain generalization of the Grüneisen parameter,  $\eta_{50}$ .

A peculiarity of the thermodynamic formulation is that although it expresses the Helmholtz energy as a function of volume and temperature, in practice it is used to compute the Gibbs energy as a function of pressure and temperature. In view of this application, we classify the parameters according to their approximate relation to the pressure-temperature derivatives of the Gibbs energy. Thus, the reference Helmholtz energy is the zeroth-order parameter,  $\theta_0$ ,  $\gamma_0$ , and  $V_0$  are most closely related to entropy and volume and considered first-order thermodynamic properties, and the remaining parameters relate to second- and third-order thermodynamic properties (e.g., expansivity and elastic moduli). With rare exception, the stable mantle phases are impure. Impure phases are described as a chemically equivalent mechanical mixture of pure end-members plus a theoretical configurational entropic term and an excess function that accounts for energetic interactions among the end-members and/or deficiencies in the entropic term. In the *Stixrude and Lithgow-Bertelloni* [2011] data base, the excess function does not depend on pressure or temperature and involves only zeroth-order parameters ( $W_{ij}$ ) that describe pair-wise interactions between end-members  $i$  and  $j$ . Although wave speeds are determined primarily by high-order properties, the low-order properties are

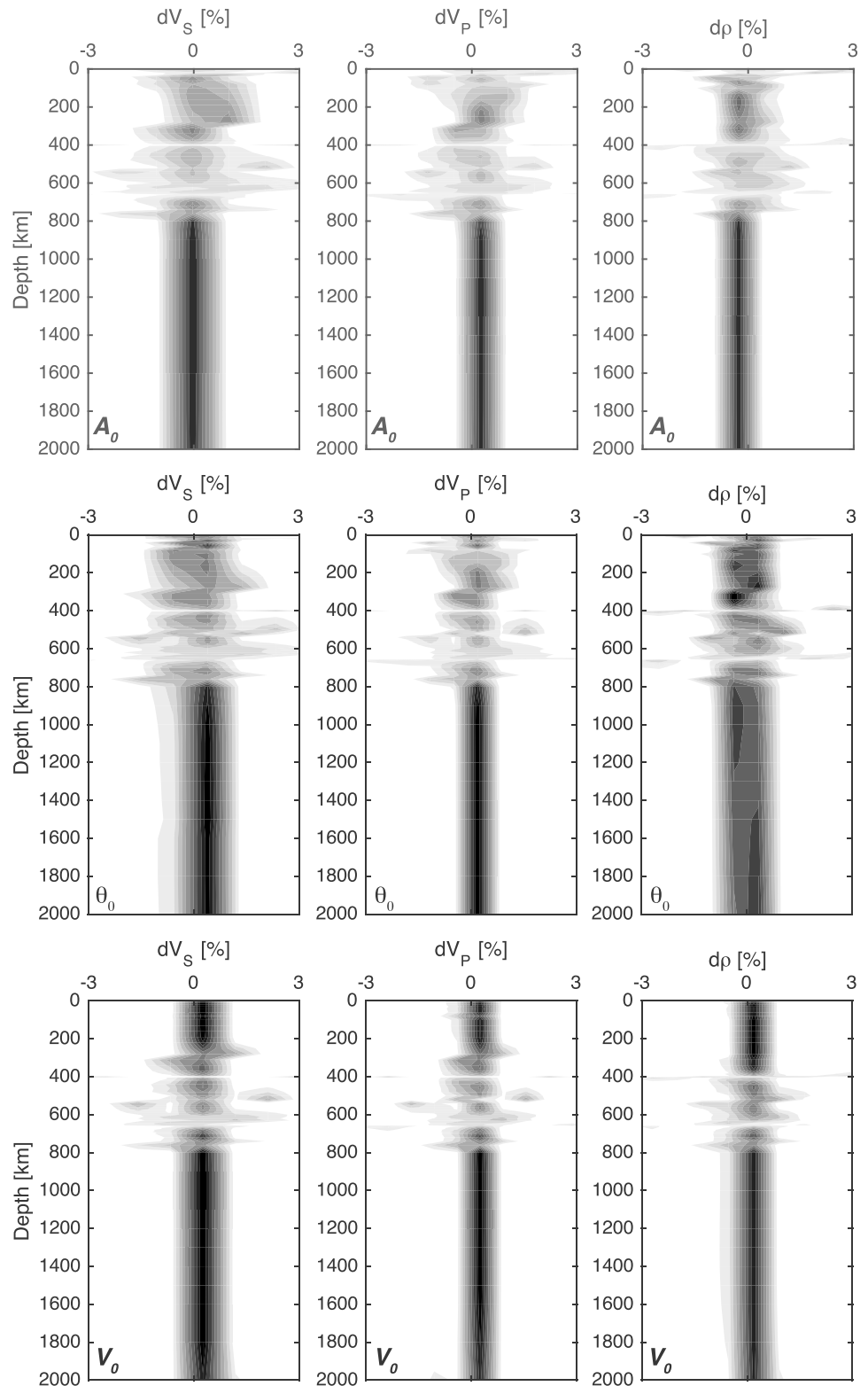


**Figure 3.** Uncertainty in  $S$  wave speed ( $dV_S$ ),  $P$  wave speed ( $dV_P$ ), and density ( $d\rho$ ) relative to the reference model (Figure 1) as a function of depth for Group 1 thermodynamic parameters. Group 1 parameters most strongly influence mineral stabilities and composition; thus, the computed uncertainties reflect the mineralogical and compositional components of the total uncertainty. Plots, from top to bottom, are the conditional uncertainties resulting from the uncertainty in  $A_0$ ,  $\theta_0$ ,  $V_0$ ,  $\gamma_0$ , and  $W_{ij}$ , respectively. Gray-scale levels indicate eight equally-sized probability density intervals for the distributions, with black indicating most probable and white least probable.

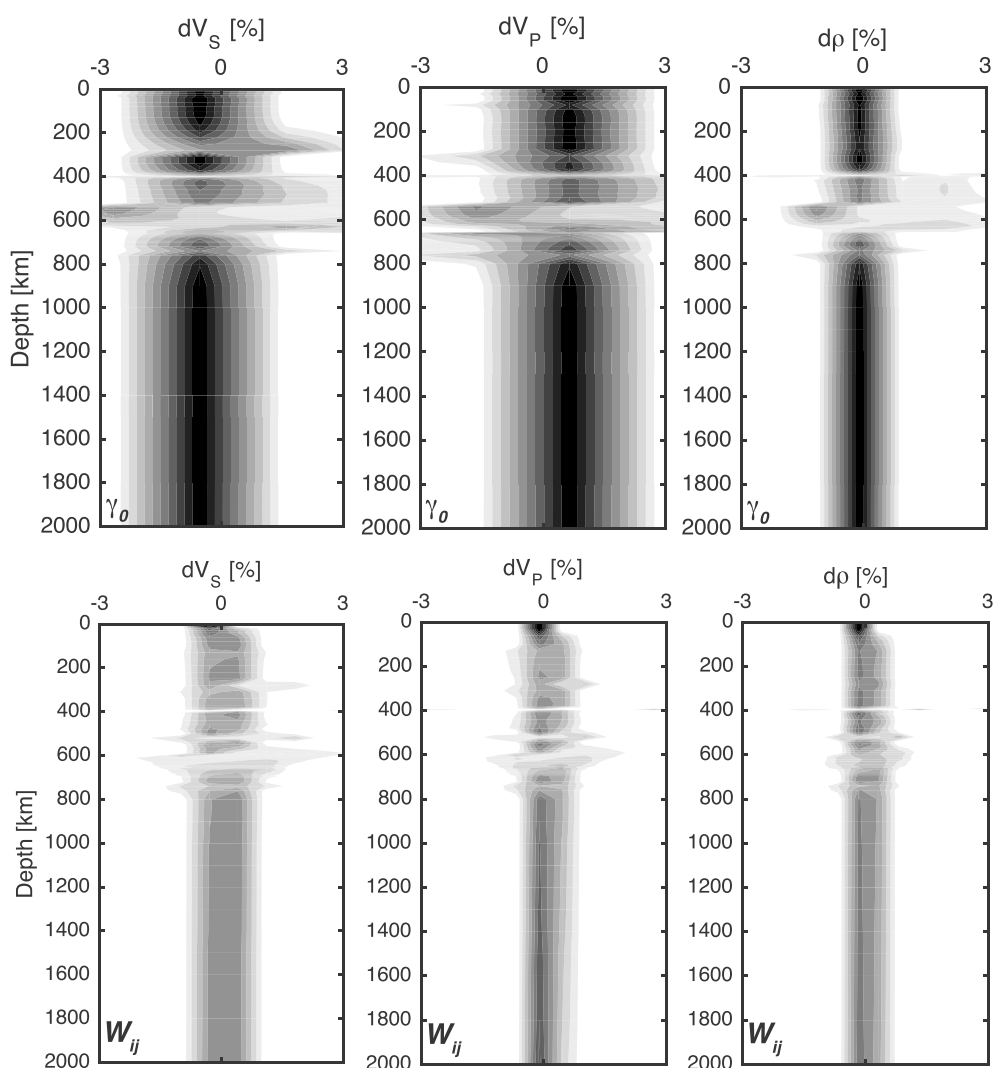
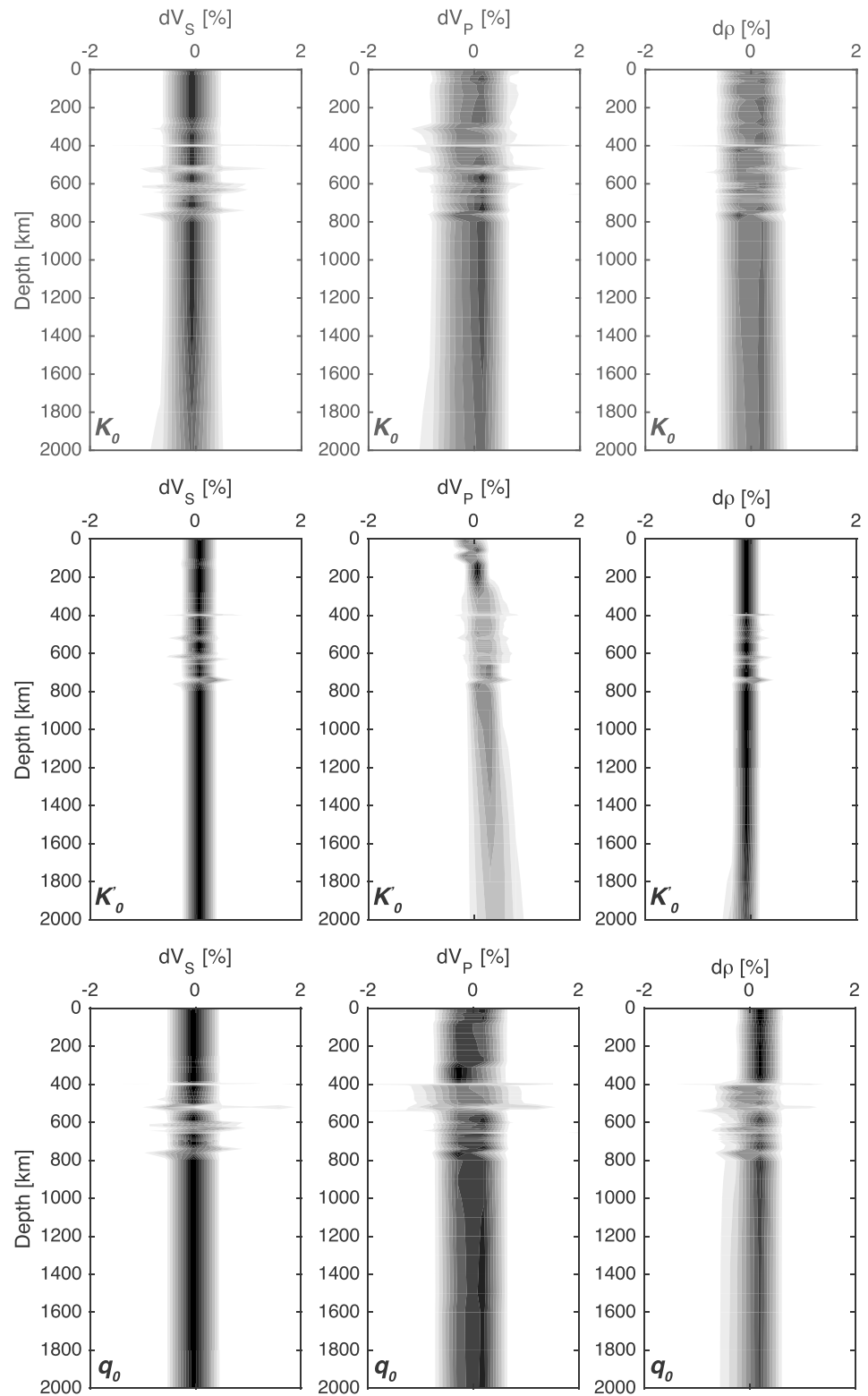


Figure 3. (continued)

critical because they determine the identity and compositions of the mineralogy predicted by Gibbs energy minimization.

*Stixrude and Lithgow-Bertelloni* [2011] do not provide covariance estimates, but uncertainties of a parameter and its direct derivative(s) tend to be strongly correlated and behave similarly [e.g., *Bass et al.*, 1981; *Bina*, 1995]. Thus, an analysis that considers the error in all 11 parameters without considering correlations will substantially overestimate the uncertainty of the predictions. To avoid this failing, we made 11 independent Monte Carlo simulations in which a single parameter was varied stochastically within its uncertainty. With the exception of  $V_0$ , the uncertainties were taken as specified by *Stixrude and Lithgow-Bertelloni* [2011]. *Stixrude and Lithgow-Bertelloni* [2011] apparently did not fit  $V_0$  by inversion and therefore give no explicit error estimate for it. For the present analysis,  $V_0$  was assumed to have a relative error of 0.25%, which is comparable to the errors in  $V_0$  assessed for mantle minerals by *Kuskov and Fabrichnaya* [1994].

The mantle pressure profile was obtained by integrating the vertical load from the surface pressure boundary condition. At lithospheric depths, temperature was computed by a prescribed geothermal gradient of 13 K/km to a depth of 100 km, the sublithospheric mantle adiabat was defined by the entropy of the lithology at a temperature of 1300 K, i.e., at the base of the lithosphere. For each stochastic analysis, we performed  $10^5$  iterations. The computed properties of the reference model for the pyrolytic bulk composition are shown in Figure 1.



**Figure 4.** Uncertainty in  $S$  wave speed ( $dV_S$ ),  $P$  wave speed ( $dV_P$ ), and density ( $d\rho$ ) relative to the reference model (Figure 1) as a function of depth for Group 2 thermodynamic parameters. Group 2 parameters strongly influence bulk modulus and density, but also affect phase equilibria and shear moduli; thus, the computed uncertainties reflect the elastic component of the total uncertainty. Plots, from top to bottom, are the conditional uncertainties resulting from the uncertainty in  $K_0$ ,  $K'_0$ , and  $q_0$ , respectively. Gray-scale levels indicate eight equally-sized probability density intervals for the distributions, with black indicating most probable and white least probable.

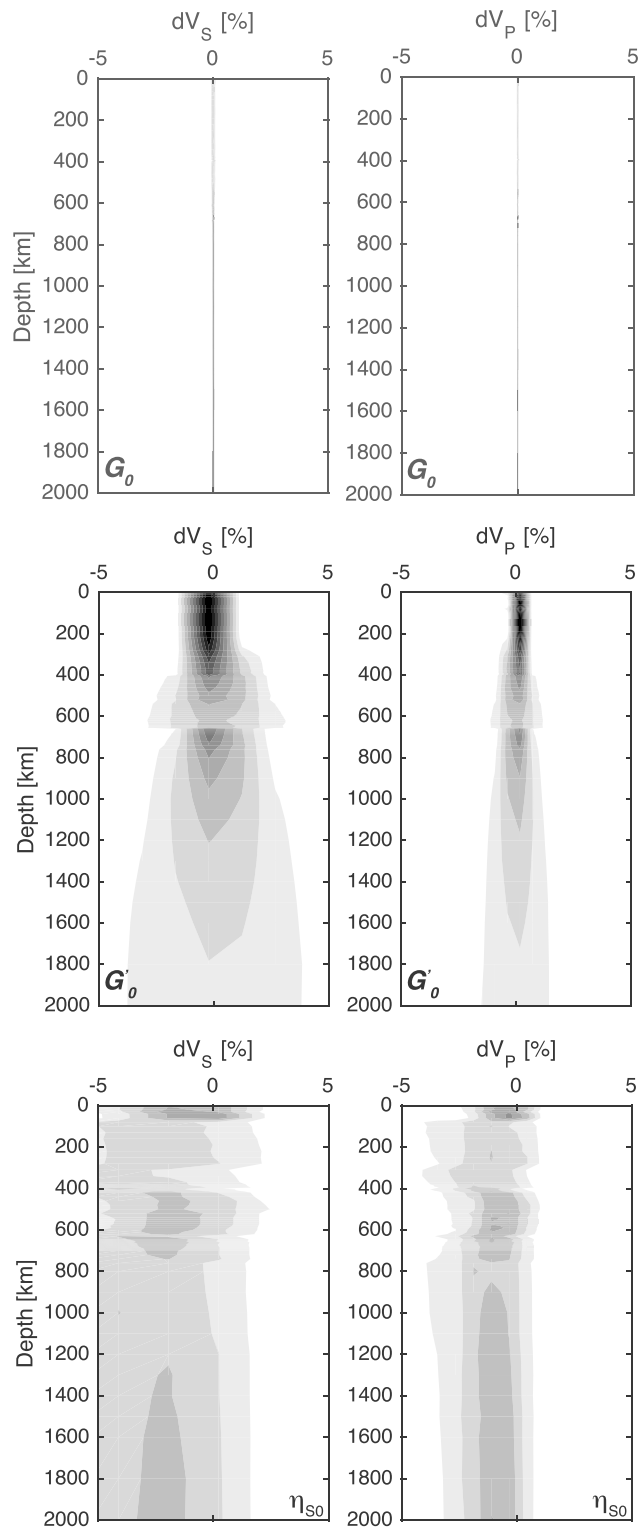


**Figure 5.** Uncertainty in  $S$  wave speed ( $dV_S$ ) and  $P$  wave speed ( $dV_P$ ) relative to the reference model (Figure 1) as a function of depth for Group 3 thermodynamic parameters. Group 3 parameters strongly influence computed shear moduli but have no influence on phase equilibria or bulk modulus. Plots, from top to bottom, are the conditional uncertainties resulting from the uncertainty in  $G_0$ ,  $G'_0$ , and  $\eta_{S0}$ . Gray-scale levels indicate eight equally-sized probability density intervals for the distributions, with black indicating most probable and white least probable.

### 3. Results and Discussion

We group parameters based on thermodynamic significance as (1)  $A_0$ ,  $\theta_0$ ,  $V_0$ ,  $\gamma_0$ , and  $W_{ij}$ ; (2)  $K_0$ ,  $K'_0$ , and  $q_0$ ; and (3)  $G_0$ ,  $G'_0$ , and  $\eta_{50}$ . Group 1 consists of zeroth- and first-order parameters that dominate the mineralogical and compositional components of the uncertainty. Group 2 consists of second- and third-order parameters that dominate the elastic component of the uncertainty, but which also influence computed phase equilibria. Group 3 consists of second- and third-order parameters that largely determine the shear modulus but have no influence on density or computed phase equilibria. For each group we show (Figures 3–5) the conditional uncertainties in wave speeds and density to a depth of 2000 km for the pyrolytic composition; comparable results are obtained for the basaltic composition (supporting information). The greatest uncertainties in the pressure and temperature of the mantle adiabat is caused by Group 1 thermodynamic parameters. Specifically, uncertainty in  $\gamma_0$  and  $A_0$  lead to relative uncertainties of  $\sim 2.5\%$  and  $\sim 0.5\%$  in, respectively, adiabatic temperature and pressure (Figure 2). That these uncertainties are greatest in the transition zone and tend to be uniform in the lower mantle suggests they primarily reflect the depth-integrated effect of transition zone mineralogical uncertainty.

The restriction to mantle depths of  $< 2000$  km permits discrimination between the mineralogical and compositional components of the conditional uncertainties in that essentially no phase transitions occur in the models at depths greater than  $\sim 800$  km, which is effectively the depth of the model upper mantle. Thus, uncertainties computed for Group 1 parameters at  $> 800$  km depth are representative of the compositional component of the conditional uncertainties, albeit strictly only for the ferropicrinite+bridgmanite+Ca-perovskite mineral assemblage. In the upper mantle mineralogical uncertainty roughly doubles Group 1 conditional uncertainties. With the exception of  $\gamma_0$ , uncertainties associated with Group 1 parameters (Figure 3) are  $\sim 2\%$  in the upper mantle,  $\sim 1\%$  in the lower mantle, and slightly greater for  $S$  wave speeds than they are for density and  $P$  wave speeds. The uncertainty associated with  $\gamma_0$  is roughly double these values. The uncertainties for Group 2 parameters (Figure 4) show comparatively little variation between the upper and lower mantle, as is consistent with the expectation that these parameters have minor influence on the identity of the stable minerals. Because constraints on elastic moduli are derived primarily from experiments at relatively low pressure and/or temperature [cf., Murakami *et al.*, 2012], it is expected that the elastic component of the uncertainty should increase systematically with depth [e.g., Stixrude and Jeanloz, 2015]. This tendency is observed for the conditional uncertainty in  $P$  wave speeds associated with  $K'_0$ , but this uncertainty is smaller than that associated with  $K_0$  and  $q_0$ . The parameter  $q_0$  also influences the extrapolation of the moduli with depth, but the absence of a systematic increase in the uncertainty associated with  $q_0$  with depth suggests that, at least for an adiabatic extrapolation, this effect is minor. For Group 2 parameters the characteristic uncertainty is  $\sim 1\%$  for both  $P$  wave speed and density throughout the mantle; the conditional uncertainties for  $S$  wave speeds from this group are lower because Group 2 parameters have little influence on the shear modulus. The relation of Group 3 parameters to shear modulus is directly analogous to the relation of Group 2 parameters to bulk modulus as borne out by the depth dependences of the respective conditional uncertainties (Figure 5). However, in Group 2 the greatest uncertainty is associated with  $K_0$ , whereas in Group 3, the smallest uncertainty is associated with  $G_0$ . Most likely, this discrepancy reflects the inversion process by which the parameters are estimated from experimental data, in that  $K_0$  is influenced by phase equilibria, but  $G_0$  is not. Given the absence of any clear correlation with depth in the conditional uncertainty associated with  $\eta_{50}$ , the uncertainties associated with Group 3 are  $\sim 4\%$  and  $\sim 2\%$  in  $S$  and  $P$  wave speeds throughout the mantle.

### 4. Conclusion

The most surprising feature of this analysis is that the mineralogical, compositional, and elastic components of the uncertainty in  $P$  wave speed are comparable. Neither the compositional nor elastic components of the uncertainty are strongly depth dependent, and, given that phase transitions are primarily a feature of the upper mantle, this behavior has the consequence that  $P$  wave speeds are most uncertain in the upper mantle. A similar pattern is observed for the uncertainty in density. In our analysis, we have divided thermodynamic parameters into groups such that we expect strong within-group and weak across-group correlations between the parameter estimates. To the extent this expectation is realized, the maximum conditional uncertainty among the parameters of a group will approximate the total uncertainty in computed properties resulting from that group, but the uncertainty arising from each group will be approximately additive. Based on this logic the total uncertainty in  $P$  wave speed computed from phase equilibrium models is  $\sim 4\%$  in the

upper mantle and ~3% in the lower mantle; the corresponding uncertainties in density are roughly 1% lower. In contrast to  $P$  wave speed and density, the elastic component of the uncertainty in  $S$  wave speed is dominant at all depths within the mantle, and the total  $S$  wave speed uncertainty is ~5% irrespective of depth.

#### Acknowledgments

We are grateful to Craig Bina and Juan Carlos Afonso for helpful and constructive reviews. This work was supported by Swiss National Science Foundation Grant 200020\_162450.

#### References

- Afonso, J. C., J. Fullea, W. L. Griffin, Y. Yang, A. G. Jones, J. A. D. Connolly, and S. Y. O'Reilly (2013), 3-D multiobservable probabilistic inversion for the compositional and thermal structure of the lithosphere and upper mantle I: A priori information and geophysical observables, *J. Geophys. Res. Solid Earth*, *118*, 2586–2617, doi:10.1002/jgrb.50124.
- Bass, J. D., R. C. Liebermann, D. J. Weidner, and S. J. Finch (1981), Elastic properties from acoustic and volume compression experiments, *Phys. Earth Planet. Int.*, *25*, 140–158.
- Bina, C. R. (1995), Confidence limits for silicate perovskite equations of state, *Phys. Chem. Minerals*, *22*, 375–382.
- Bina, C. R. (1998), Free energy minimization by simulated annealing with applications to lithospheric slabs and mantle plumes, *Pure Appl. Geophys.*, *151*, 605–618.
- Birch, F. (1952), Elasticity and constitution of the Earth's deep interior, *J. Geophys. Res.*, *57*(2), 227–286.
- Cammarano, F. (2013), A short note on the pressure-depth conversion for geophysical interpretation, *Geophys. Res. Lett.*, *40*, 4834–4838, doi:10.1002/grl.50887.
- Cammarano, F., S. Goes, P. Vacher, and D. Giardini (2003), Inferring upper-mantle temperatures from seismic velocities, *Phys. Earth Planet. Inter.*, *138*, 197–222, doi:10.1016/s0031-9201(03)00156-0.
- Cammarano, F., B. Romanowicz, L. Stixrude, C. Lithgow-Bertelloni, and W. Xu (2009), Inferring the thermochemical structure of the upper mantle from seismic data, *Geophys. J. Int.*, *179*, 1169–1185.
- Cobden, L., S. Goes, M. Ravenna, E. Styles, F. Cammarano, K. Gallagher, and J. A. D. Connolly (2009), Thermochemical interpretation of 1-D seismic data for the lower mantle: The significance of nonadiabatic thermal gradients and compositional heterogeneity, *J. Geophys. Res.*, *114*, B11309, doi:10.1029/2008JB006262.
- Connolly, J. A. D. (2009), The geodynamic equation of state: What and how, *Geochem. Geophys. Geosyst.*, *10*, Q10014, doi:10.1029/2009GC002540.
- Connolly, J. A. D., and D. M. Kerrick (2002), Metamorphic controls on seismic velocity of subducted oceanic crust at 100–250 km depth, *Earth Planet. Sci. Lett.*, *204*, 61–74.
- Drilleau, M., E. Beucler, A. Mocquet, O. Verhoeven, G. Moebs, G. Burgos, J.-P. Montagner, and P. Vacher (2013), A Bayesian approach to infer radial models of temperature and anisotropy in the transition zone from surface wave data, *Geophys. J. Int.*, *195*, 1165–1183, doi:10.1093/gji/ggt284.
- Dziewonski, A. M., and D. L. Anderson (1981), Preliminary reference earth model, *Phys. Earth Planet. Inter.*, *25*, 297–356, doi:10.1016/0031-9201(81)90046-7.
- Fabrichnaya, O., S. K. Saxena, P. Richet, and E. F. Westrum (2004), *Thermodynamic Data, Models, and Phase Diagrams in Multicomponent Oxide Systems*, 198 pp., Springer, Berlin, doi:10.1007/978-3-662-10504-7.
- Ganguly, J., A. M. Freed, and S. K. Saxena (2009), Density profiles of oceanic slabs and surrounding mantle: Integrated thermodynamic and thermal modeling, and implications for the fate of slabs at the 660 km discontinuity, *Phys. Earth Planet. Int.*, *172*, 257–267, doi:10.1016/j.pepi.2008.10.005.
- Ita, J., and L. Stixrude (1992), Petrology, elasticity, and composition of the mantle transition zone, *J. Geophys. Res.*, *97*, 6849–6866.
- Jackson, I. (1998), Elasticity, composition and temperature of the Earth's lower mantle: A reappraisal, *Geophys. J. Int.*, *134*, 291–311.
- Kennett, B. L. N., and I. Jackson (2009), Optimal equations of state for mantle minerals from simultaneous non-linear inversion of multiple datasets, *Phys. Earth Planet. Inter.*, *176*, 98–180, doi:10.1016/j.pepi.2009.04.005.
- Khan, A., J. A. D. Connolly, and N. Olsen (2006), Constraining the composition and thermal state of the mantle beneath Europe from inversion of long-period electromagnetic sounding data, *J. Geophys. Res.*, *111*, B10102, doi:10.1029/2006JB004270.
- Khan, A., L. Boschi, and J. A. D. Connolly (2009), On mantle chemical and thermal heterogeneities and anisotropy as mapped by inversion of global surface wave data, *J. Geophys. Res.*, *114*, B09305, doi:10.1029/2009JB006399.
- Kuskov, O. L., and O. B. Fabrichnaya (1994), Constitution of the moon. 2. Composition and seismic properties of the lower mantle, *Phys. Earth Planet. Inter.*, *83*, 197–216, doi:10.1016/0031-9201(94)90089-2.
- Kuskov, O. L., V. A. Kronrod, A. A. Prokofyev, and N. I. Pavlenkova (2014), Thermo-chemical structure of the lithospheric mantle underneath the Siberian craton inferred from long-range seismic profiles, *Tectonophysics*, *154*, 615–616, doi:10.1016/j.tecto.2014.01.006.
- Mattern, E., J. Matas, Y. Ricard, and J. Bass (2005), Lower mantle composition and temperature from mineral physics and thermodynamic modeling, *Geophys. J. Int.*, *160*, 973–990, doi:10.1111/j.1365-246X.2004.02549.x.
- Matas, J., J. Bass, Y. Ricard, E. Mattern, and M. S. T. Bukowski (2007), On the bulk composition of the lower mantle: Predictions and limitations from generalized inversion of radial seismic profiles, *Geophys. J. Int.*, *170*, 764–780, doi:10.1111/j.1365-246X.2007.03454.x.
- Murakami, M., Y. Ohishi, N. Hirao, and K. Hirose (2012), A perovskitic lower mantle inferred from high-pressure, high-temperature sound velocity data, *Nature*, *485*, 90–94, doi:10.1038/nature11004.
- Piazzoni, A. S., G. Steinle-Neumann, H. P. Bunge, and D. Dolejs (2007), A mineralogical model for density and elasticity of the Earth's mantle, *Geochem. Geophys. Geosyst.*, *8*, Q11010, doi:10.1029/2007GC001697.
- Saxena, S. K., and G. Eriksson (1983), Theoretical computation of mineral assemblages in pyrolyte and lherzolite, *J. Petrol.*, *24*, 538–555.
- Sobolev, S. V., and A. Y. Babeyko (1994), Modeling of mineralogical composition, density and elastic-wave velocities in anhydrous magmatic rocks, *Surv. Geophys.*, *15*, 515–544.
- Stixrude, L., and R. Jeanloz (2015), Constraints on seismic models from other disciplines—Constraints from mineral physics on seismological models, in *Treatise on Geophysics, Volume 1: Seismology and the Structure of the Earth*, vol. 1, 2nd ed., edited by G. Schubert, pp. 829–852, Elsevier, Amsterdam, doi:10.1016/B978-0-444-53802-4.00022-1.
- Stixrude, L., and C. Lithgow-Bertelloni (2005), Thermodynamics of mantle minerals—I. Physical properties, *Geophys. J. Int.*, *162*, 610–632, doi:10.1111/j.1365-246X.2005.02642.x.
- Stixrude, L., and C. Lithgow-Bertelloni (2011), Thermodynamics of mantle minerals—II. Phase equilibria, *Geophys. J. Int.*, *184*, 1180–1213, doi:10.1111/j.1365-246X.2010.04890.x.
- Thio, V., L. Cobden, and J. Trampert (2016), Seismic signature of a hydrous mantle transition zone, *Phys. Earth Planet. Int.*, *250*, 46–63, doi:10.1016/j.pepi.2015.11.005.
- Wood, B. J., and J. R. Holloway (1984), A thermodynamic model for subsolidus equilibria in the system CaO-MgO-Al<sub>2</sub>O<sub>3</sub>-SiO<sub>2</sub>, *Geochim. Cosmochim. Acta*, *66*, 159–176.